THE GEOLOGICAL SOCIETY OF AMERICA

Identification of Fugitive Dust Generation, Transport, and Deposition Areas Using Remote Sensing

WILLIAM L. STEFANOV

Department of Geological Sciences and Center for Environmental Studies, Arizona State University, Tempe, AZ 85287-6305

MICHAEL S. RAMSEY

Department of Geology and Planetary Science, 200 SRCC Building, University of Pittsburgh, Pittsburgh, PA 15260

PHILIP R. CHRISTENSEN

Department of Geological Sciences, Arizona State University, Tempe, AZ 85287-6305

Key Terms: ***Fugitive Dust, Remote Sensing, Air Quality, ETM+, Land-Cover Classification, Expert System, Particulates, Atmospheric (Circulation) Modeling***

ABSTRACT

Fugitive (or airborne) dust is a primary cause of decreased air quality, as well as being a potential health hazard. Urban and agricultural areas are of particular interest as fugitive dust sources because of their potential for releases during soil disturbance, ongoing industrial and commercial processes, and agricultural activities. Typical strategies for assessing and monitoring fugitive dust source areas include numerical modeling of atmospheric circulation patterns, field assessments, and collection of dust samples using various methods. Analysis of remotely sensed multi-spectral data provides another alternative for identifying fugitive dust source, transport, and sink areas. Multi-spectral (visible to shortwave infrared) data acquired by the Enhanced Thematic Mapper Plus (ETM+) instrument on board the Landsat 7 satellite is used to perform land-cover classifications for the Nogales, AZ, region. Data acquired during the winter of 2000 and the summer of 2001 are used to assess seasonal variations and detect land-cover changes of significance to dust-transport processes. An expert system approach using spectral, textural, and vegetation abundance data is used to classify the ETM+ data into land-cover types important to dust-transport models. The determined overall accuracy of the land-cover classifications is 74 percent. These results can be used to identify (and calculate areal percentages of) fugitive dust source, transport, and sink regions. This spatially explicit, digital data product is useful both as an input into dust-transport models and as a check on the results of such models.

INTRODUCTION

Fugitive Dust

Airborne, or fugitive, dust is identified as a potential health hazard in the United States under the Clean Air Act Amendments of 1990. Specifically, the fraction of silt- to clay-sized particulates ranging from 0 to 10 μm in diameter is used as a regulatory standard for the determination of air quality (Chow et al., 1992). Fugitive dust originates from anthropogenic (combustion of fossil fuels, vehicular traffic, industrial emissions, pesticide and herbicide applications) and natural (windblown soil and unpaved road dust) sources (Péwé et al., 1981; Iskander et al., 1997), many or all of which can be found in association with urban centers in the southwestern United States and northern Mexico. Differing levels of regulatory control in the two countries also create a situation wherein airborne pollutants generated in Mexico can cross the border into the United States (and vice versa).

Fugitive dust studies in the literature typically focus on field-based data collection for epidemiological and elemental analyses. Specific substances of interest can include mineralogical/elemental components (Péwé et al., 1981; Danin and Ganor, 1997; Iskander et al., 1997; and Gómez et al., 2001); endotoxins and allergens (Ezeamuzie et al., 1998; Miguel et al., 1999; and Nieuwenhuijsen et al., 1999); and pesticides (Simcox et al., 1995). There is also a large body of work in the geological literature regarding the dynamics of airborne dust generation, transport, and deposition (Lancaster and Nickling, 1994).

Numerical dispersion and atmospheric circulation models, such as the Environmental Protection Agency Urban Airshed Model IV (UAM-IV) and the Pennsylvania State University/National Center for Atmospheric Research Mesoscale Model Five (MM5), are employed to estimate atmospheric and pollutant transport dynamics using ground-based observations of meteorological, particulate, and land-cover data (Scheffe and Morris, 1993; Chen and Dudhia, 2001a, 2001b). The meteorological and particulate data are usually acquired on a near real-time basis, but land-cover inputs to these models are frequently obtained from spatially averaged or out-of-date information, which can lead to errors in model outputs (J. Zehnder, personal communication, August 24, 2001). Remote sensing and classification of land-cover types important to fugitive dust generation, transport, and deposition presents a potential source of moderate- to high-resolution, spatially explicit, and temporally accurate data for input into numerical transport and dispersion models.

Remote Sensing and Land-Cover Classification

Surficial materials (rocks, soils, vegetation, asphalt, etc.) reflect, transmit, or re-emit some percentage of incident energy at different wavelengths because of electronic transitions, molecular rotations, and vibration of chemical bonds (Kahle et al., 1993). The science of remote sensing is concerned with the detection and measurement of reflected and emitted energy from the surface of the Earth (and other planets). The wavelength regions of use in terrestrial remote sensing are defined by atmospheric windows and include the visible to near infrared (0.4–0.9 μm), shortwave infrared (0.9–3.0 μm), and mid-infrared (3.0–5.0 and 8.0–14.0 μm). Satellite and airborne remote sensing instruments sensitive to these wavelength ranges are 'passive' in that ambient solar radiation is the primary source of energy incident to the ground surface, rather than the sensor itself (Sabins, 1997). Plotting the variations of detected energy with wavelength produces spectra that can be used to obtain specific identifications of surficial materials (spectroscopy).

Studies of the distribution of surficial materials (or land cover) on a regional to global scale have been conducted since 1974 using visible to near-infrared multispectral data collected by sensors on board the Landsat series of satellites at ground resolutions of 30–80 m/pixel (Sabins, 1997). The most recent sensor in the Landsat series, the Enhanced Thematic Mapper Plus (ETM+) on board the Landsat 7 satellite, retains the visible to shortwave-infrared wavelength coverage and spatial resolution (30 m/pixel) of the preceding Thematic Mapper instruments. In addition, a 15-m/pixel panchromatic band and improved resolution mid-infrared band (60 m/pixel, with high- and low-gain channels) have been incorporated into the sensor (Irish, 1998).

The data volume inherent in multi-spectral remotely sensed data (such as those collected by the ETM+) can be collapsed and made more meaningful to end users through the use of statistical clustering algorithms. These algorithms classify individual pixels into discrete populations based on analysis of the variability of information within the dataset and automated determination of class means (unsupervised classification). Supervised classification algorithms allow for user specification of spectral class means through the use of training pixels derived from the dataset or spectral libraries. Supervised algorithms make use of *a priori* knowledge of a given remotely sensed scene, and therefore they tend to be somewhat more accurate than unsupervised classifications (Jensen, 1996). Both unsupervised and supervised algorithms are 'hard' classifiers in that they assign each pixel into one specific class only.

The primary data source for urban remote sensing since 1974 has been readily available and frequently acquired multi-spectral information from a succession of satellite-based sensors exemplified by the Landsat and Système Probatoire d'Observation de la Terre programs. Accurate discrimination of land-cover types in urban/exurban areas using these data and traditional unsupervised and supervised classification techniques is difficult because of high spatial heterogeneity at the pixel level. This difficulty is compounded by high degrees of subpixel mixing, especially along boundaries between different land-cover types (Ridd, 1995; Foody, 2000). This produces a mixed spectral signature that is difficult to classify accurately using hard classification algorithms. A successful technique for improvement of classification accuracy is to combine other forms of geospatial information with remotely sensed surficial properties data (Trietz, 1992; Harris and Ventura, 1995; Vogelmann et al., 1998; Stuckens et al., 2000; and Stefanov et al., 2001). These additional data layers can then be used in hypothesis-testing models (also known as expert systems) to obtain accurate land-cover classifications. Geospatial data useful in constraining traditional spectral-based land-cover classifications in urban/exurban areas include secondary remotely sensed information such as vegetation indices and spatial texture. Integration of sociopolitical and environmental data available through geographic information systems (GIS) and remotely sensed surficial data for most cities is expected to become a standard technique for urban (and environmental) analysis (Donnay et al., 2001).

Research Objectives

The primary research objective was to identify land-cover types of interest to fugitive dust modeling using

remotely sensed data. Data collected by the ETM+ sensor were selected for this purpose because they are readily available for the U.S.–Mexico border region, provide moderately high spatial resolution (30 m/pixel), are acquired approximately every 14 to 16 days, and have spectral coverage useful for identification of both natural and built surficial materials. Stefanov and others (2001) used an expert system to accurately classify a wide variety of land-cover types (active and fallow agricultural fields; cultivated grass; undifferentiated vegetation; fluvial and lacustrine sediments; water; undisturbed desert; and a range of disturbed surfaces including xeric and mesic residential built materials, commercial/industrial built materials, and asphalt/concrete) in the Phoenix, AZ, region using Landsat Thematic Mapper (the predecessor of the ETM+) data. This expert system has been modified for use in the Nogales, AZ, region to classify land-cover types associated with fugitive dust generation, transport, and deposition. The ultimate goal of the research is to provide spatially explicit, digital land-cover data with moderately high ground resolution for input into dust-transport models. A secondary goal is to develop remote sensing techniques for fugitive dust research and modeling that can be easily modified for use with higher spatial and spectral resolution sensors such as the Advanced Spaceborne Thermal Emission and Reflection Radiometer (ASTER), currently orbiting on the Terra satellite (Abrams, 2000).

The Nogales, AZ, area was selected as the study site for this work because it is an urban area located along the U.S.–Mexico border region (Figure 1). The implementation of the North American Free Trade Agreement in 1994 significantly accelerated economic growth in the border region, with subsequent increases in population growth (current population is 12 million people; this number is expected to double by 2020), industrial facilities, and cross-border traffic. Air and water pollution has also increased in the region, leading to more intensive efforts to characterize and monitor pollution sources and sinks (Ganster et al., 2000).

A recent assessment of air quality in the Nogales, AZ, and Nogales, Sonora, region performed by the Arizona Department of Environmental Quality (ADEQ) identified unpaved dirt roads as a significant contributor to elevated levels of fugitive dust (Heisler et al., 1999). Increasing density of unpaved roads and construction sites associated with urban growth in the region leads to the creation of new non-industrial or combustion-related fugitive dust sources on a short temporal time scale due to land-cover change. As such, this area presents an ideal situation for use of remotely sensed data and testing of the expert system technique. Secondary research objectives included comparison of ETM+ pixel spectra with field reflectance spectra as an accuracy assessment tool and land-cover change detection in the field area using bi-

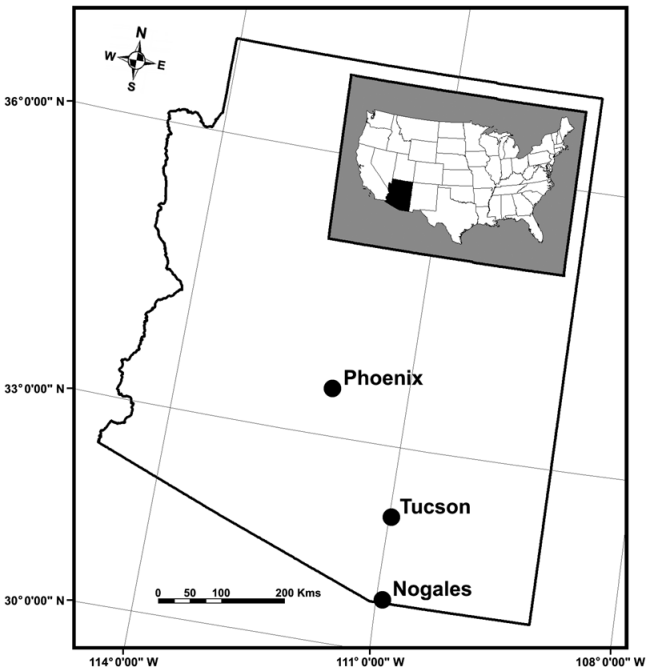

Figure 1. Location map for the study area, with black circles indicating the major urban centers of southern Arizona and Nogales, AZ.

seasonal ETM+ data. Figure 2 illustrates the general physiography (both natural and human) of the field area and presents photographs of representative fugitive dust generation, transport, and deposition land-cover types.

METHODOLOGY

Processing of Remotely Sensed Data

Two ETM+ scenes were obtained from the U.S. Geological Survey's EROS Data Center for the study area to allow for change detection analysis. The dates of scene acquisition (November 22, 2000, and June 2, 2001) were selected in order to capture winter and summer seasonal conditions. Each scene was georeferenced to the WGS 84 spheroid and Universal Transverse Mercator Zone 12 North coordinate system. The two scenes were co-registered to each other to within 0.5 pixel (15 m) using differential Geographic Positioning System (GPS) road network data collected in the field. The study area was extracted from each scene, corrected for the effects of atmosphere, and converted to calibrated reflectance using commercially available software that incorporates the Moderate Resolution Atmospheric Transmittance and Radiance code (Geosystems GmbH, 1999). An arid atmosphere, desert aerosol concentration model with 15 km estimated visibility was used as input to the radiative transfer code for both scenes.

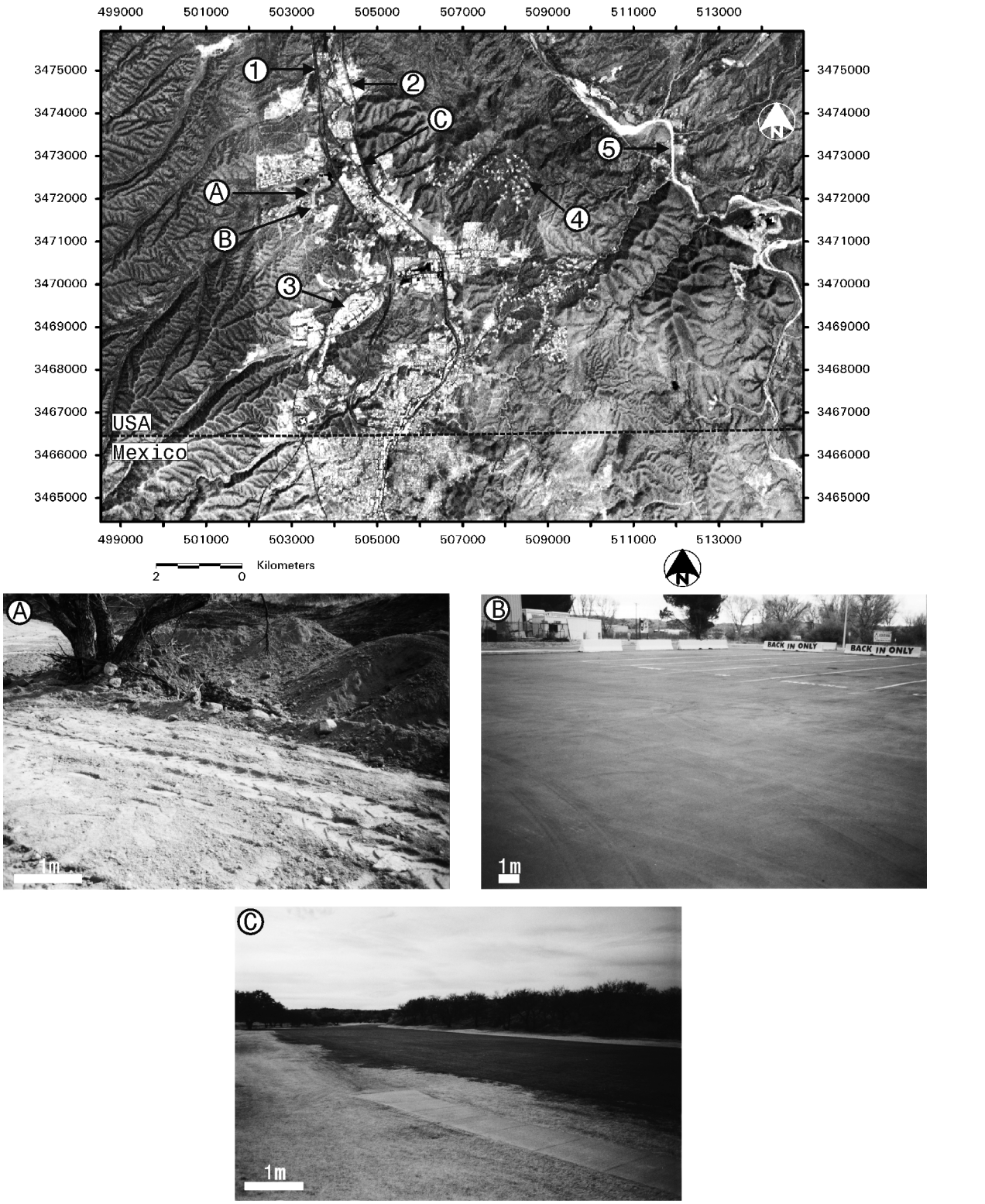

Figure 2. Enhanced Thematic Mapper Plus panchromatic image acquired on June 2, 2001, of the study area, with the dashed line indicating the U.S.–Mexico border (note that this and all subsequent images are projected in geographic coordinates of Universal Transverse Mercator with the WGS 84 datum). Major human and natural physiographic features are indicated for reference to subsequent figures: Interstate Highway 19 (1), U.S. Route 89 (2), commercial/industrial facilities (3), hillside residential area (4), and the Santa Cruz River bed (5). Photographs depict representative fugitive dust generation (A: residential construction site), transport (B: asphalt parking lot), and deposition (C: golf course) land-cover types.

Calculation of Vegetation Index

Vegetation abundance for each pixel was calculated for both ETM+ scenes using the Soil-Adjusted Vegetation Index (SAVI) of Huete (1988). This index compares the reflectance values in the visible-red and near-infrared portions of the electromagnetic spectrum. Actively photosynthesizing vegetation has a reflectance peak in the near-infrared (ETM+ band 4) and low reflectance in the visible-red portion of the spectrum (ETM+ band 3). The vegetation index data are used as an additional source of surficial information in the expert system model because they provide a simple numerical measure of the degree of vegetation abundance on a per-pixel basis. This information helps to limit potential mis-classification of vegetated areas due to sub-pixel mixing (Stefanov et al., 2001). The SAVI is similar to the frequently used Normalized Difference Vegetation Index (Botkin et al., 1984) but includes an additional factor to account for soil reflectance such that one obtains

$$SAVI = \left[\frac{(NIR - VISred)}{(NIR + VISred + L)}\right] \cdot (1 + L) \qquad \text{Eq. 1}$$

where NIR = near-infrared band (band 4) and $VISred$ = visible-red band (band 3). The factor L in Equation 1 is designed to correct for the soil reflectance component of energy detected by the sensor and is set at 0.5 (Huete, 1988). The calculated SAVI values were rescaled to 0–255 for incorporation into the expert system model. Figure 3 presents the SAVI image derived from the summer ETM+ data.

Calculation of Variance Texture

The study area comprises urbanized, undisturbed, and grazing regions. These different types of land uses have distinct spatial edge frequencies (or spatial texture) that can be used as input into classification algorithms (Irons and Petersen, 1981; Gong and Howarth, 1990; and Stuckens et al., 2000). Urban areas typically have significant texture resulting from buildings and street grids, whereas homogeneous areas such as large grazing fields have little to no texture (Figure 4). Inclusion of spatial texture into the expert classifier therefore provides a useful discriminator of urban versus nonurban regions that is helpful in identifying fugitive dust generation, transport, and deposition areas. Texture values were calculated from the ETM+ base data using a 3×3 moving window and the variance equation

$$Variance = \sum \frac{(x_{ij} - M)^2}{n - 1} \qquad \text{Eq. 2}$$

where x_{ij} = Digital Number value of pixel (i,j), n = number of pixels in the moving window, and M = the mean pixel value of the moving window (ERDAS, 1999):

$$M = \frac{\Sigma x_{ij}}{n} \qquad \text{Eq. 3}$$

The 15-m/pixel panchromatic ETM+ band was not used in spatial texture analysis, because natural surfaces exhibit significant texture at this resolution (making urban versus nonurban area discrimination much more difficult).

Image Classification

Land-cover classes of interest were determined based on association with fugitive dust generation, transport, and depositional processes. These associations were determined primarily on the basis of existing geological theory regarding the production, mobilization, and deposition of windborne particles (Lancaster and Nickling, 1994); field observations in the study area; and the results of an air quality assessment performed by the ADEQ in the study area (Heisler et al., 1999). Soil surfaces disturbed because of urban growth (construction activities and creation of dirt roads), grazing, and recreational off-road vehicle use are major dust generation areas. Many impervious and non-vegetated urban surfaces such as parking areas, industrial buildings, sidewalks, and paved roadways can act as regions of dust transport because of the low surface roughness and increased wind velocity associated with these land-cover types. Dust can also be generated from paved roadways because of vehicular traffic; however, field observations indicated that fine particulates were rapidly removed from paved roadways by surface winds. Therefore, we have placed impervious urban surfaces into the transport grouping of land-cover types. Heavily vegetated areas such as riparian zones and golf courses will act as dust deposition sites because of the increased surface roughness and corresponding drop in wind velocity. Anthropogenic sources of particulate matter, such as industrial processes and fossil fuel combustion, are not included in our analyses because the ETM+ sensor is not optimally configured to detect them. Table 1 lists the land-cover classes used in the initial classification of ETM+ data and their associated roles in fugitive dust processes.

Training regions for the land-cover classes were determined using geological, land-use, and site-visit data. Training pixels for the land-cover classes were obtained for both the summer and winter ETM+ scene, with the only exception being the Water class. Training pixels for this class were obtained from the winter scene only, because appreciable water was not present in the summer scene. Each training region consisted of at least 60 image pixels to satisfy the $10n$ criterion, where n = number of bands used for the classification (Jensen, 1996). Multiple

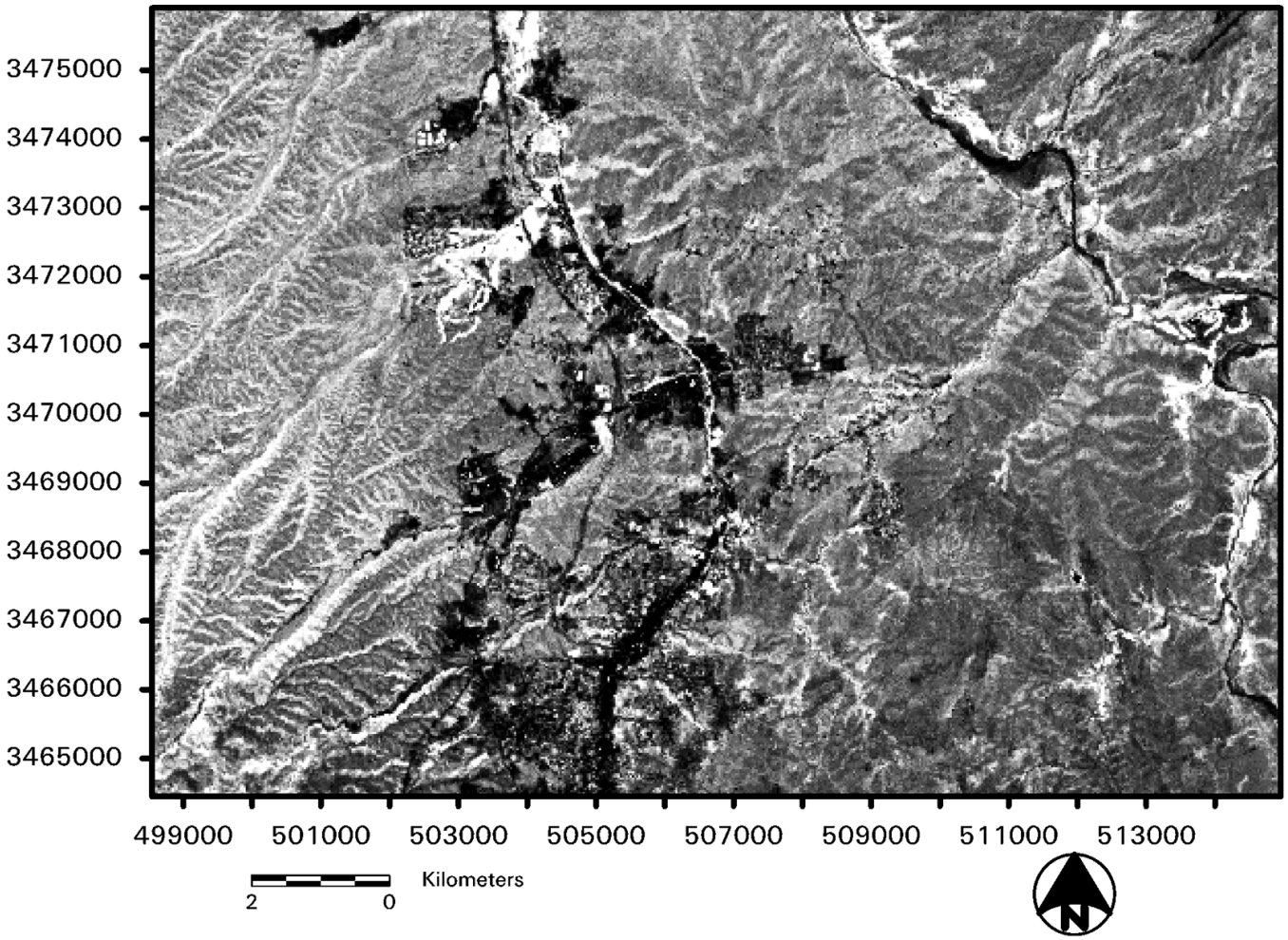

Figure 3. Relative abundance of actively photosynthesizing vegetation was determined for both winter and summer datasets (summer data shown) using Equation 1. Bright pixels are dominated by vegetation, with dark pixels having little to no vegetation.

training regions were selected for each class and then merged to ensure a Gaussian distribution of pixel values. Training region statistics were calculated for each class and are presented as image spectra in Figure 5. A hard classification of the ETM+ data was then performed using a maximum likelihood rule. Maximum likelihood rules define a specific data volume for each class based on the image pixel statistics. This classification rule is more accurate than minimum distance algorithms, which classify pixels based solely on their proximity to calculated class means (Jensen, 1996).

The relative accuracies of standard supervised classification approaches such as minimum distance, maximum likelihood, and fuzzy classification are assessed for the Phoenix metropolitan area using Landsat TM data by Stefanov and others (2001). The results of their study indicated that the best classification performances were attained using fuzzy classification and maximum likelihood techniques (70 to 72 percent overall accuracy) with a relatively small number of land-cover classes (four). Because of the similarity in land-cover types between Nogales, AZ, and Phoenix, AZ, a similar analysis was not performed for the study area. The results of Stefanov and others (2001) also demonstrate the advantages of incorporating additional datasets into an expert system framework for classification of urban/exurban areas (overall classification accuracy of 85 percent for the Phoenix, AZ, metropolitan area with 12 land-cover classes).

An expert system classification model was constructed using commercial image-processing software (ERDAS Imagine 8.4; ERDAS, 1999) and implemented on a Unix-based Sun Ultra 2 server. The primary motivation behind using the expert system was to reclassify the initial maximum likelihood classification using the SAVI and image texture information. This was done to reduce errors of omission (all pixels of a given class not correctly identified) and commission (all pixels of a given class correctly identified, plus other pixels incorrectly identified as that class). Use of the expert system also allowed for the recoding of the Hillslope (shadowed) and Open

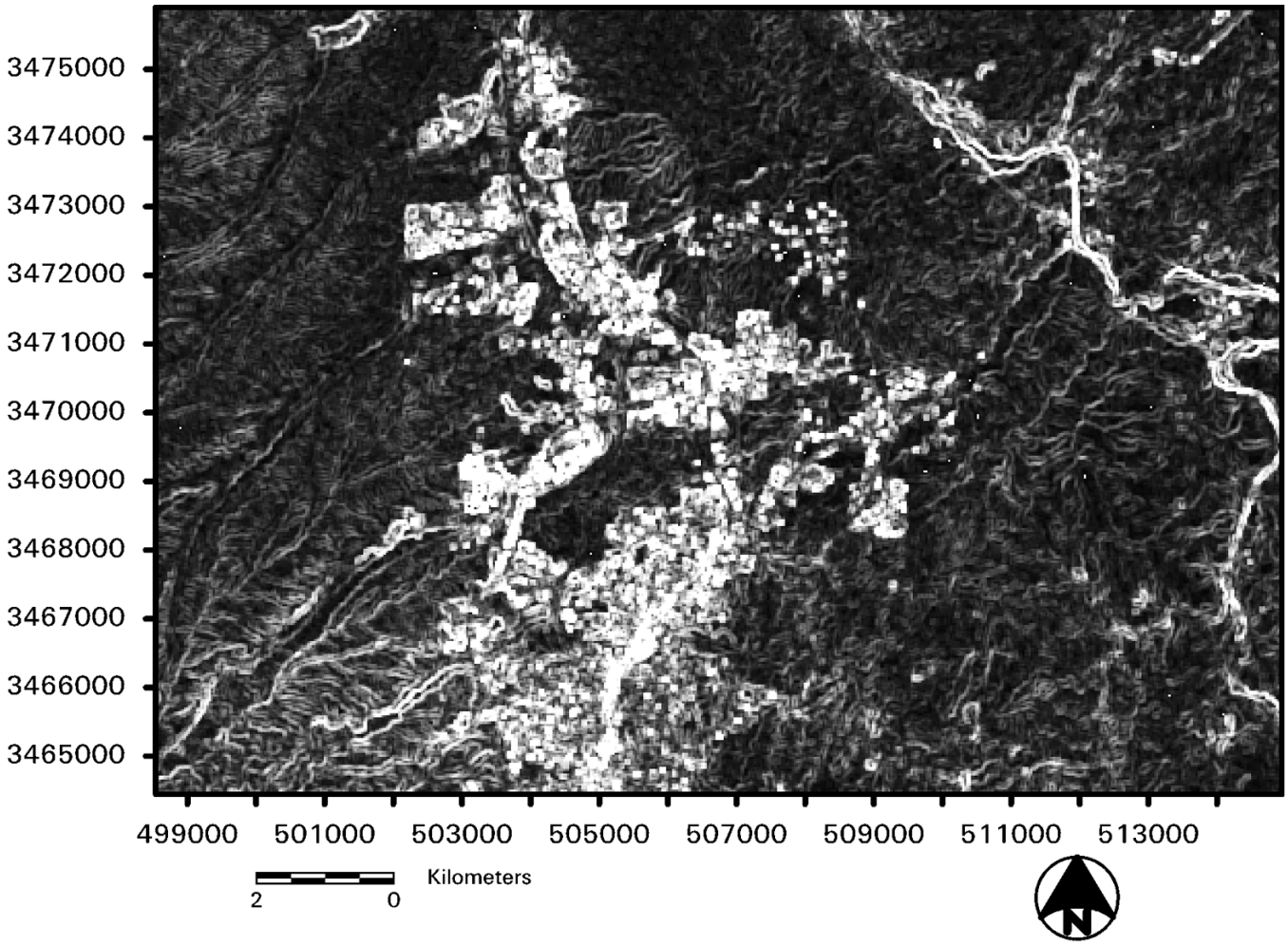

Figure 4. Spatial variance texture was calculated from Enhanced Thematic Mapper Plus bands 2 and 5 for both winter and summer datasets (summer data shown) using Equations 2 and 3. Bright pixels correspond to areas with high proportions of edges, such as urbanized regions. Dark pixels correspond to areas with little to no edges, such as golf courses and hillsides. Natural linear features (such as ridges and stream washes) are detected using this method, but the calculated variance values tend to be lower than those for urban regions.

Field classes in the initial land-cover classification to the Undisturbed and Vegetation classes, respectively. Several other classes were renamed as well: Undisturbed (low vegetation) to Undisturbed; Disturbed (commercial/industrial) to Urban (commercial/industrial); Disturbed (mixed urban) to Urban (mixed); Disturbed (asphalt + concrete) to Asphalt + Concrete; and Cultivated Vegetation to Vegetation (cultivated). Definitions of the expert system classes are provided in Table 2.

Pixel classifications were determined using a hypothesis-testing framework (Figure 6). In this schematic figure, the dashed rectangle indicates the hypothesis for evaluation, diamonds indicate decision pathways, and rectangles indicate the variables to be tested. A pixel will receive the final hypothesized classification if the conditional variables comprising any decision pathway are true. For example, if a pixel is initially classified as Disturbed (asphalt + concrete), has a spatial variance texture value in ETM+ band 5 (1.55–1.75 μm) greater than 10, and has a SAVI value greater than or equal to 120, the pixel is reclassified as Undisturbed. Only data derived from the remotely sensed imagery were used in

Table 1. *Initial land cover classes for the maximum likelihood rule.*

Class	Role in Dust Process
Hillslope (shadowed)	Generation
Bare Soil	Generation
Undisturbed (low vegetation)	Generation
Disturbed (commercial/industrial)	Transport
Disturbed (mixed urban)	Transport
Disturbed (asphalt + concrete)	Transport
Undisturbed (high vegetation)	Deposition
Open Field	Deposition
Cultivated Vegetation (golf courses, watered lawns)	Deposition
Water	Deposition

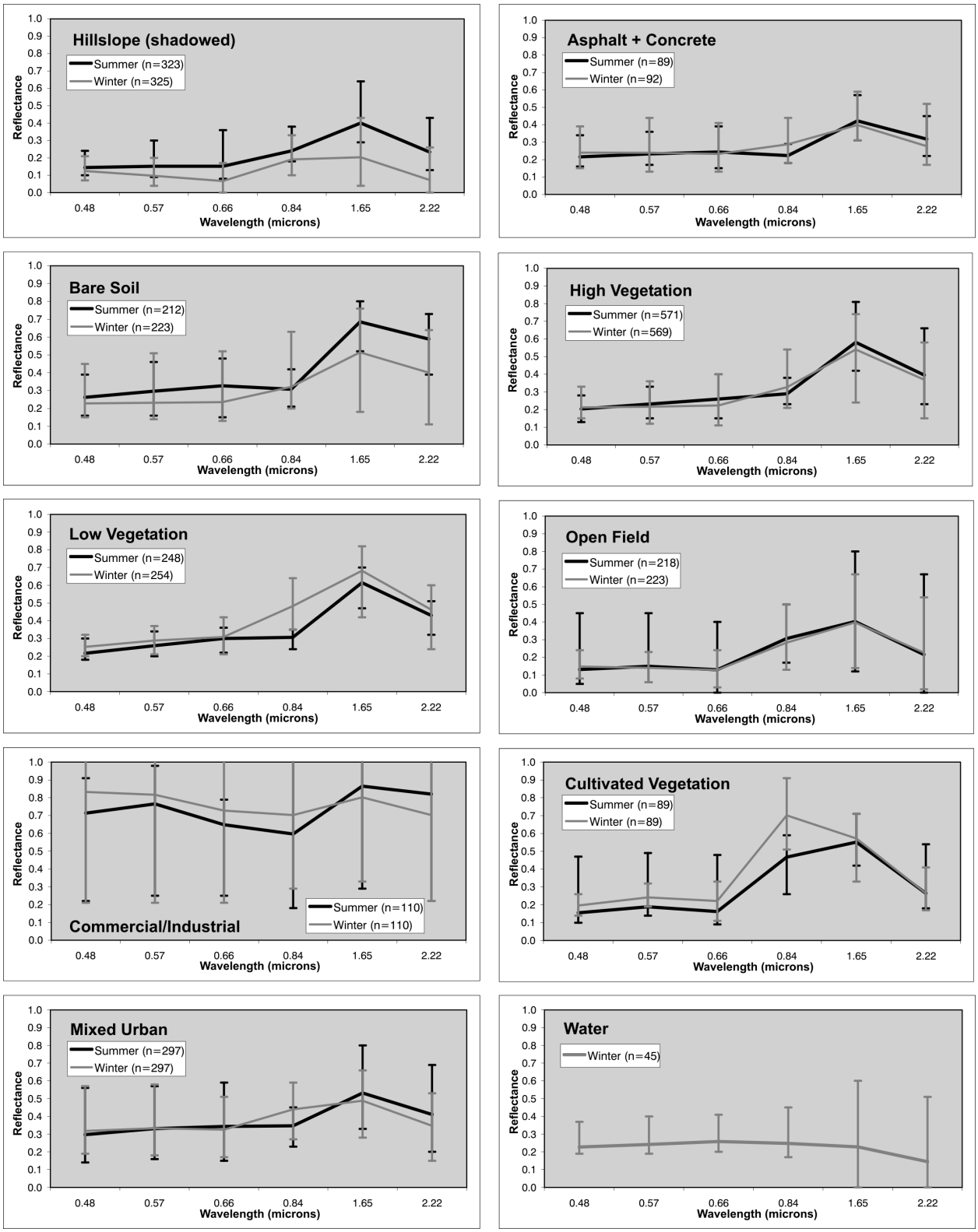

Figure 5. Training region statistics for the winter (gray curves) and summer (black curves) land-cover types used in the initial maximum likelihood classifications are presented as averaged Enhanced Thematic Mapper Plus (ETM+) pixel reflectance spectra. The number of pixels comprising each winter and summer class training region is given as *n*. Differences in *n* between winter and summer scenes are due to redefinition of training regions (primarily to reflect seasonal differences in vegetation density and location). Error bars denote minimum and maximum reflectance values for each ETM+ band.

Table 2. *Class definitions for the expert system model.*

Class	Properties
Undisturbed	Undisturbed soil and sparse vegetation, bedrock outcrops
Bare Soil	Soil with title to no vegetation, dry stream washes, disturbed and graded soil
Urban (commercial/industrial)	Mixed asphalt, concrete, soil, and building materials; high spatial texture
Urban (mixed)	Mixed asphalt, concrete, soil, vegetation, and building materials; high spatial texture
Asphalt + Concrete	Mixed asphalt and concrete
Undisturbed (high vegetation)	Undisturbed soil with abundant vegetation
Vegetation	Actively photosynthesizing vegetation
Vegetation (cultivated)	Actively photosynthesizing cultivated grass (golf courses and watered lawns)
Water	Standing or flowing water

the present work because of a dearth of ancillary data for the study area. The classification hypotheses and test parameters used in the expert model are presented in Appendix A. Each pixel is tested by each hypothesis in a sequential fashion. As each pixel is classified according to the hypothesis it satisfies, the model requires only a single pass through the data.

Field Reflectance Spectral Collection

Reflectance spectra were collected from several training regions and other sites in the Nogales, AZ, study area during a winter field campaign (December 10–11, 2000) using an Analytical Spectral Devices Fieldspec Handheld (FH) field spectrometer. The FH acquires absolute reflectance spectra from 0.264 to 1.074 μm using a Spectralon calibration target. This spectral range corresponds to bands 1–4 of the ETM+ sensor, allowing comparisons of on-the-ground measurements with the remotely sensed data. Such comparisons are useful in verifying training region spectra obtained from the ETM+ data. A total of 48 field spectra of various surficial materials was collected during the winter field campaign. Field spectral collection locations were reoccupied (when possible) during a subsequent summer (June 9–11, 2001) field campaign. An additional 43 spectra were collected during the summer field campaign. Field validation of training sites used in both the winter and summer land-cover classifications was also performed during each field campaign.

The following procedure for collection of field reflectance spectra was standardized as much as possible

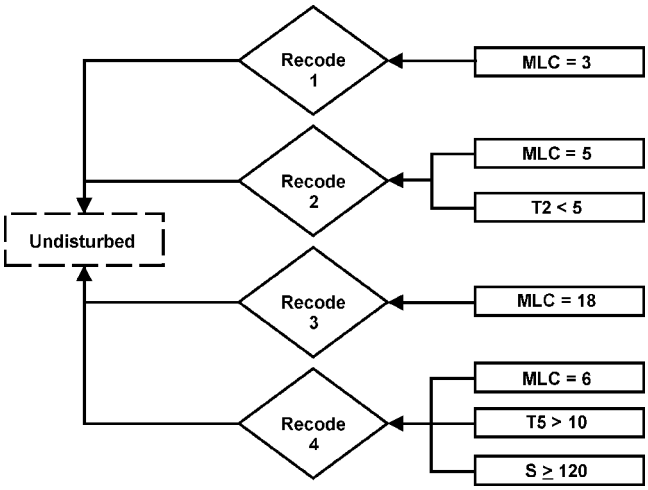

Figure 6. Schematic example diagram of the expert system used to produce final land-cover classifications for the study area. The dashed rectangle represents the hypothesis being tested, diamonds are conjunctive decision rules, and solid rectangles represent the variables being tested (on a pixel basis). Variable definitions are: MLC = maximum likelihood classification result (values are defined in Appendix A); T2 = spatial variance texture value for Enhanced Thematic Mapper Plus (ETM+) band 2; T5 = spatial variance texture value for ETM+ band 5; S = SAVI value. Multiple branches connected to a single hypothesis are exclusive conditional statements.

to ensure collection of comparable data during each field campaign. A calibration spectrum was acquired from the Spectralon target prior to collection of the target spectrum (or spectra). During the winter field campaign, variable atmospheric conditions (cloud cover) necessitated frequent collection of calibration spectra. Atmospheric conditions during the summer campaign were clear and sunny, which allowed for the collection of fewer calibration spectra. Where physically possible, four spectra were collected at the vertices of a 30-m × 30-m area to simulate an ETM+ pixel. Spectra of areally dominant surficial materials were collected in areas where the preceding protocol was not possible. The physical location of each spectral collection site was recorded using a GPS unit, and photographs of the site were taken. Figure 7 presents representative field and corresponding image pixel spectra for the major land-cover types of interest (corresponding to the field photographs in Figure 2). Field spectra have been degraded to ETM+ resolution using the sensor filter functions. The field and image pixel spectra were acquired during the winter field campaign and winter ETM+ scene, respectively.

RESULTS

The present research effort uses the experimental design of Stefanov and others (2001) for land-cover classification of semi-arid to arid urban centers. Figures 8 and 9 present the expert system land-cover classifications

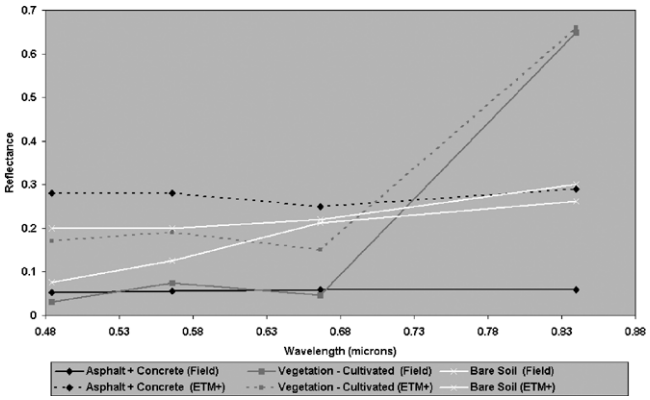

Figure 7. Field reflectance spectra (solid curves) were collected during both the winter and summer field campaigns for comparison to Enhanced Thematic Mapper Plus (ETM+) image pixel spectra (dashed curves). Spectra for three land-cover classes corresponding to fugitive dust generation (Bare Soil), transport (Asphalt + Concrete), and deposition (Vegetation [cultivated]) are presented (see Figure 2). Agreement between field and image pixel spectra is good, with absolute reflectance differences due mainly to scale differences between the two types of measurements (4.45-cm spot diameter for field spectra versus a 30-m × 30-m ETM+ image pixel).

for the November 2000 and June 2001 ETM+ scenes, respectively. Classification accuracy was assessed for the summer scene using a reference dataset of 598 randomly selected points for which land cover was determined using an August 1998 digital aerial orthophoto mosaic (1-m/pixel resolution) georeferenced to the ETM+ data. The original ETM+ data were also used in accuracy assessment to avoid introducing errors into the reference dataset for temporally sensitive classes (such as bare soil regions related to construction activities). The expert

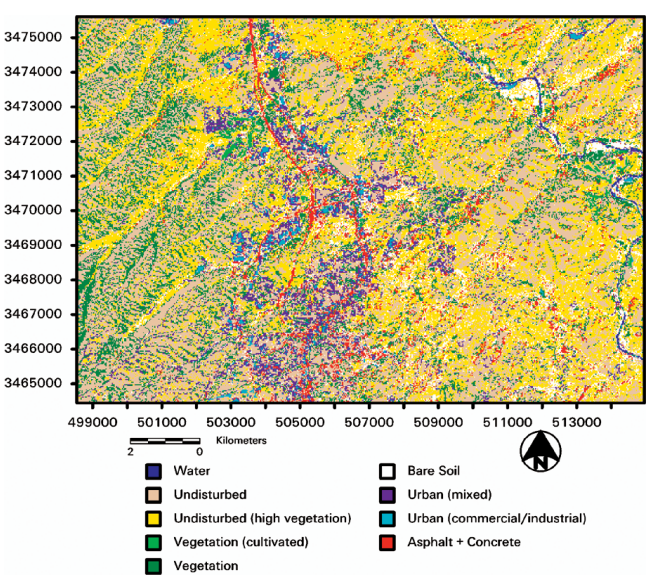

Figure 8. Land-cover classification derived from the winter Enhanced Thematic Mapper Plus data using the expert system.

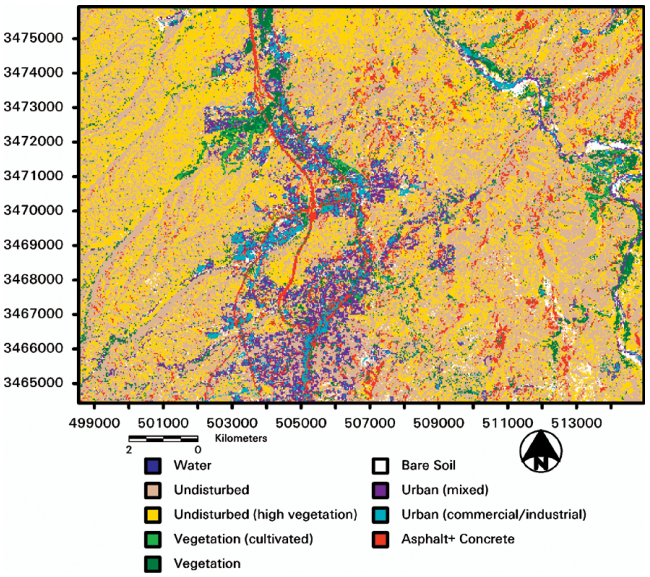

Figure 9. Land-cover classification derived from the summer Enhanced Thematic Mapper Plus data using the expert system.

system land-cover classifications were used to generate 100 random validation points for each output class. An automated 3 × 3 pixel filter was passed over the output classifications to determine validation points and ensure random selection of each point.

A simple class majority rule was used with the filter in order to maximize the likelihood of selecting validation points within contiguous class groupings rather than isolated (and potentially mis-classified) pixels. Validation pixels that fell within their own class training regions were removed from the reference dataset. Likewise, validation points that did not have pixel values equal to the class under inspection (an artifact of the pixel selection method) were discarded. This resulted in a range of 60–73 validation points for each output class. Of the total reference points, 538 were selected using the summer scene; the remaining 60 points (associated with the water class) were selected from the winter scene. This was done because there were few water pixels in the summer scene, whereas the winter scene contained numerous water pixels. Additional land-cover data for the reference dataset were collected by field verification of the classified images during both the winter and summer field campaigns.

Both producer's accuracy (the percentage of pixels classified as a particular land cover that actually are that land cover) and user's accuracy (the percentage of reference pixels for a given land cover that are correctly classified) are generally reported. User's accuracy is the more relevant measure of a classification's actual accuracy in the field. Additional information regarding the error matrix can be obtained using a conditional Kappa analysis, which incorporates measures of the

Table 3. *Accuracy assessment for expert system classification.*

Class	Reference Totals	Classified Totals	No. Correct	Producer's Accuracy (%)	User's Accuracy (%)	Kappa (%)
Water	57	60	57	100.00	95.00	0.00
Undisturbed	117	70	58	49.57	82.86	78.09
Undisturbed (high vegetation)	77	71	59	76.62	83.10	80.28
Vegetation (cultivated)	55	65	53	96.36	81.54	79.44
Vegetation	66	61	53	80.30	86.89	85.05
Bare Soil	97	61	53	54.64	86.89	84.04
Urban (mixed)	48	64	39	81.25	60.94	57.20
Urban (commercial/industrial)	44	73	41	93.18	56.16	52.36
Asphalt + Concrete	37	73	32	86.49	43.84	39.69
Totals	598	598	445			
Overall classification accuracy = 74.41 percent						
Overall Kappa = 68.16 percent						

omission and commission errors to obtain accuracy values (Jensen, 1996). Producer's, user's, and overall accuracy (and corresponding conditional Kappa analysis values) of the summer classification were calculated using an error matrix (Congalton and Green, 1999). Accuracy assessment was performed only for the summer scene classification to minimize potential errors resulting from seasonal variation from the reference dataset (which was compiled using digital orthophotos acquired during August 1998). The winter scene classification was used to obtain accuracy assessment results for the water class. Overall classification accuracy is 74 percent (conditional Kappa accuracy of 68 percent). The results of accuracy assessment for each individual class are presented in Table 3. Table 4 lists the areal percentages of each class for both the winter and summer land-cover classifications.

Change analysis of the two ETM+ scenes was accomplished using difference images. Subtraction of the summer from the winter land-cover classification for specific classes allows for a graphical representation of the change between the two images (Figure 10). Changes in pixel classification from winter to summer (or vice versa) result from changes in the spectral character of the pixel because of significant surficial material change. For example, a pixel area with abundant vegetation classified as Vegetation (cultivated) in the winter scene may be dominantly bare soil in the summer (and classified as Bare Soil). Difference images were calculated for the Bare Soil (Figure 10A) and Undisturbed (high vegetation) classes (Figure 10B). An additional Urban 'class' difference image (Figure 10C), composed of pixels classified as Urban (mixed), Urban (commercial/industrial), and Asphalt + Concrete, was also calculated. Pixels classified as a particular land-cover type in each image were recoded to have common pixel values; all other pixels were recoded to a value of zero. The recoded images were then subtracted from each other.

DISCUSSION

Examination of the accuracy assessment results (Table 3) indicates a distinct division (in terms of accuracy) between natural and built land-cover types. User's accuracy results for the Water, Undisturbed, Undisturbed (high vegetation), Vegetation, Vegetation (cultivated), and Bare Soil classes range from 81 to 95 percent (78 to 85 percent Kappa values). The Kappa value of 0.00 for the Water class indicates that no errors of omission or commission were associated with this class. In contrast, the user's accuracy results for the Urban (mixed), Urban (commercial/industrial), and Asphalt + Concrete classes range from 44 to 61 percent (40 to 57 percent Kappa values). The overall classification accuracy is 74 percent (68 percent Kappa value).

Recasting these results in terms of fugitive dust processes (Table 4) leads to user's accuracies of 83 to 89 percent (generation sites), 81 to 95 percent (deposition sites), and 44 to 61 percent (transport sites). Comparison of the results presented in Table 4 indicate that significant changes in land-cover areal extent took place between November 2000 and June 2001. The most significant of

Table 4. *Areal percentages of land cover classes.*

Class	Fugitive Dust Process	Winter Scene (%)	Summer Scene (%)
Water	Deposition	0.46	0.06
Undisturbed (high vegetation)	Deposition	33.37	34.65
Vegetation (cultivated)	Deposition	0.51	1.05
Vegetation	Deposition	13.85	5.44
Undisturbed	Generation	32.85	41.14
Bare Soil	Generation	7.73	2.57
Urban (mixed)	Transport	5.32	6.19
Urban (commercial/industrial)	Transport	1.15	2.55
Asphalt + Concrete	Transport	4.77	6.35
Total		100.00	100.00

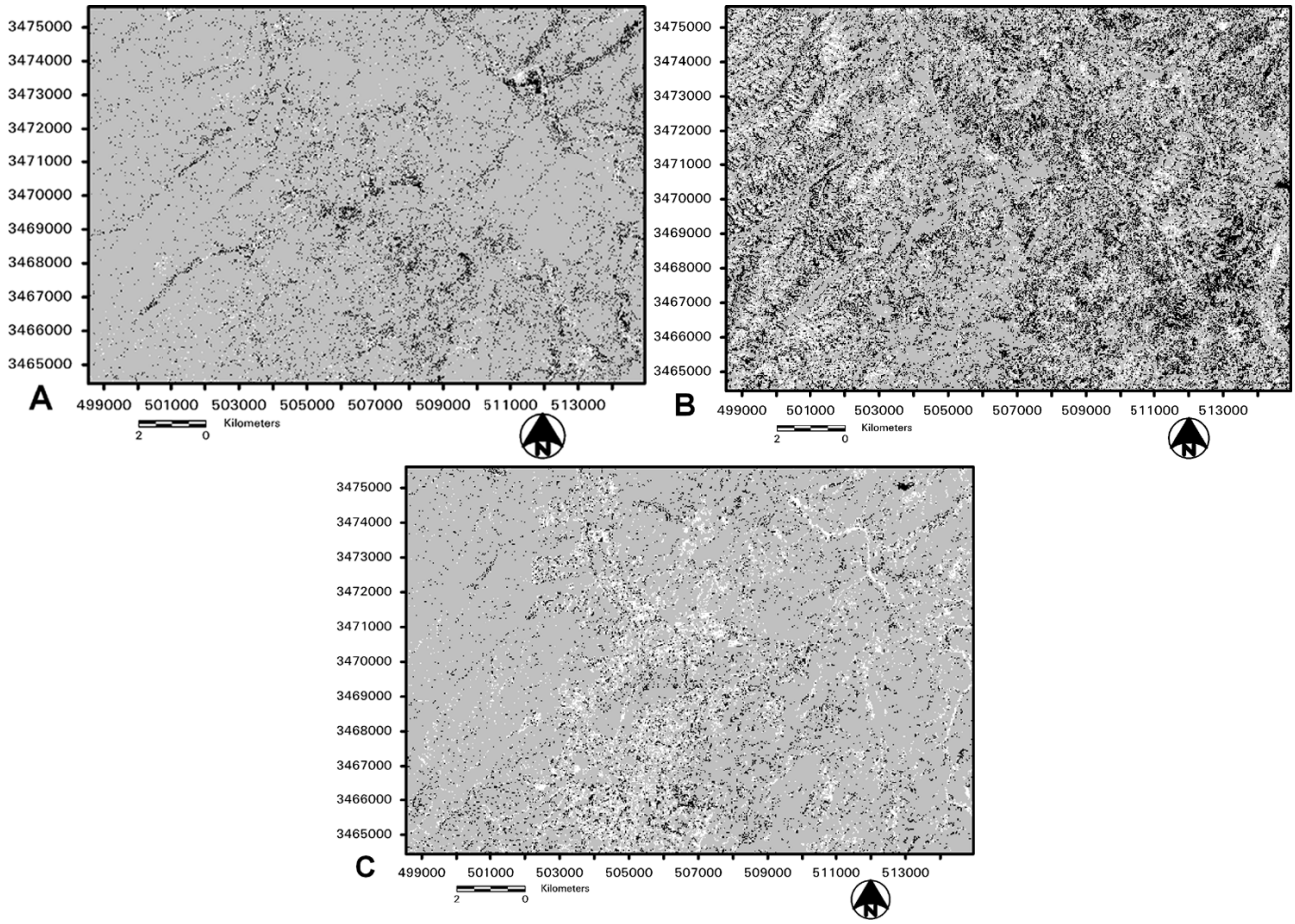

Figure 10. Change detection images were derived by subtraction of the summer classification image from the winter classification image for three land-cover classes representative of fugitive dust generation (A: Bare Soil), deposition (B: Undisturbed [high vegetation]), and transport (C: ''Urban'' [described in text]) areas. White pixels were classified as the land-cover type of interest in the summer scene, but not the winter scene; black pixels were classified as the land-cover type of interest in the winter scene, but not the summer scene; and gray pixels were not classified as the land-cover type of interest in either the winter or the summer scene.

these changes took place in the Undisturbed, Vegetation, Water, and Bare Soil classes. These classes are most likely to change spatially and spectrally during different seasons because of changes in grass cover and precipitation (MacMahon, 1988). The relative direction of the areal percentage changes for these classes is in good agreement with this conclusion, suggesting that natural fugitive dust source and sink areas are also seasonally dependent.

The results of change detection analyses (Figure 10A, B, and C) for the study area indicate that there is significant variation in the spatial location of pixels classified as Bare Soil, Undisturbed (high vegetation), and all Urban land-cover types. These particular classes were selected for analysis because they are representative of fugitive dust generation, deposition, and transport areas. Seasonal variations in the spectral character of surficial materials (mainly due to presence or absence of photosynthesizing grasses) can account for much of this variation. The variation observed in the Urban class is more problematic, however, because the spectral character of these classes should not be seasonally dependent following atmospheric correction. Slight mis-registration errors between the two classified images (on the order of 0.5 pixel) could account for the large magnitude of change observed in Figure 10C. Mis-classification of the Urban (mixed) and Asphalt + Concrete class in particular (discussed below) could account for much of the variation observed in Figure 10C.

Urban (or built) land-cover types tend to be difficult to classify accurately using hard classification techniques because of the high degree of sub-pixel mixing associated with the urban environment (Foody, 2000; Stefanov et al., 2001). Inspection of the class training area means and minimum/maximum values for both the winter and summer maximum likelihood classifications (Figure 5) indicates that considerable overlap exists between the Urban (mixed) class and other land-cover classes. This is because the Urban (mixed) class contains many of the same surficial materials that comprise the other land-

cover classes (Table 2). The correspondence between field and ETM+ spectra for homogeneous surficial materials is good (Figure 7), with major differences resulting from scale variations between the two types of measurements (4.45-cm-diameter spot for the field spectrometer versus a 30-m × 30-m ETM+ pixel). This suggests that the low classification accuracies for the built land-cover classes are a result of sub-pixel mixing rather than poor training site selection. Fuzzy classification techniques are designed to address the sub-pixel mixing problem by assigning multiple classifications to each pixel, which are ranked in order of probability (Foody, 2000). Application of a fuzzy classifier to the Phoenix, AZ, urban area by Stefanov and others (2001) did not produce significant increases in classification accuracy. The land-cover types in Nogales and Phoenix are generally similar, and therefore fuzzy classification was not performed as part of the present work.

Classification accuracy for the Asphalt + Concrete class is particularly poor (44 percent), with the majority of error resulting from confusion with the Bare Soil and Undisturbed classes (Figure 5). Visual comparison of both the field and ETM+ spectra (Figure 7) supports this conclusion, because the spectral features of the Bare Soil and Asphalt + Concrete classes are similar. Road-grade asphalt usually contains approximately 95 percent aggregate, composed of sand- to gravel-sized minerals and rocks that are typically locally derived (Brown et al., 1989). It is unknown whether or not this is true for the study area, but it could explain the observed spectral similarity between the geological materials and asphalt. Similar spectral confusion between river gravels and asphalt in the Phoenix, AZ, area was overcome by incorporating a GIS coverage that masked out the river gravel deposits (Stefanov et al., 2001). However, a similar dataset is not available for the Nogales study area.

Landsat ETM+ data has moderately high spatial resolution (30 m/pixel) in six reflective spectral bands (four in the visible to near infrared and two in the shortwave infrared). The use of remotely sensed data with higher spatial and spectral resolution could improve both the classification accuracy and mapping detail for fugitive dust-related land-cover types. Data collected by the NASA ASTER sensor span the visible to near-infrared (three bands at 15 m/pixel), shortwave infrared (six bands at 30 m/pixel), and mid-infrared (five bands at 90 m/pixel) wavelengths (Abrams, 2000). Multi-spectral shortwave infrared and mid-infrared data in particular would enhance the ability to classify disturbed soil regions such as construction sites, dirt roadways, and agricultural fields (Ben-Dor et al., 1999). Zhu and Blumberg (2002) demonstrate high land-cover classification accuracy in the Beer Sheva, Israel, metropolitan area using visible to shortwave infrared ASTER data. The methodology presented here was developed for use with ETM+ data primarily because of the wide spatial and temporal coverage of Landsat data (as compared with ASTER data). However, the expert system model can be modified for use with any remotely sensed dataset.

CONCLUSIONS

We demonstrate the application of remotely sensed data for identification and mapping of land-cover types associated with fugitive dust generation, transport, and deposition in the Nogales, AZ, region. The associations between land-cover types and dust processes presented here provide a useful framework for assessment of the classification results, and we consider them reasonably accurate based on previous regulatory investigations in the study area and field observations. However, more detailed field work and integration of our results into atmospheric models is required to confirm the land-cover/fugitive dust connections we postulate here. Further air quality assessments along the U.S.–Mexico border are planned by the ADEQ. These will allow us to test the assumptions of our methodology (in terms of dust generation and transport sites) and assess the predictive power of the technique (for dust deposition sites).

This work uses moderately high ground resolution, multi-spectral data acquired by the ETM+ sensor on board the Landsat 7 satellite; however, the technique described here can be applied to higher-resolution (both spatial and spectral) remotely sensed data as well. An expert system (or hypothesis-testing) classification model was employed to classify land cover in the study area. The expert system land-cover classification performed well for classes associated with fugitive dust generation and deposition (85 to 95 percent user accuracy). Classification performance was less satisfactory for fugitive dust transport classes (44 to 61 percent). This disparity in results is caused mainly by sub-pixel mixing of built classes and similarity to local surficial materials, as well as the lack of useful ancillary data for the study area. Change detection analyses indicate that the majority of land-cover change in the study area is due to seasonal variations in the presence of vegetation (most probably grasses and herbaceous cover). This result implies that the location of airborne dust generation and deposition areas may have a significant seasonal dependence that can be quantified using temporal series of remotely sensed data. The accuracy of classification results presented here could be improved by the incorporation of ancillary GIS data. Inclusion of such data (census, zoning, vegetation, and soil maps) would enable more sophisticated post-classification sorting of land-cover classifications derived from remotely sensed imagery. Use of higher spatial and spectral resolution remotely sensed data would also increase the ability to identify and

delineate land-cover types (particularly soil types and vegetation cover) associated with fugitive dust processes.

The land-cover classifications presented here are useful for identification of potential ''hot spots'' that can aid in focusing further field investigation, sampling efforts, and dust control measures. The identification of potential fugitive dust generation and deposition areas is likely to be of greatest importance to atmospheric scientists, government regulators, and health officials. Therefore, our technique is useful for first-order modeling of fugitive dust processes despite the low classification accuracy of the transport classes. The digital and spatially explicit format of the land-cover classification maps are also ideal for input into existing air quality and atmospheric transport models, such as the UAM-IV and the MM5. The moderately high-resolution land-cover data produced using our technique are an improvement over the coarse spatial resolution data these models typically use and can be used in a reference mode to compare with the output of air quality and dust-transport models.

ACKNOWLEDGMENTS

The authors thank Terri Wilson, U.S. Bureau of Reclamation, Phoenix Area Office, for digital aerial orthophotos of the field area used for accuracy assessment. Theresa Rigney, Randy Sedlacek, and Thomas Summers of the Arizona Department of Environmental Quality provided information on fugitive dust modeling and regulatory concerns. Jeff Mihalik (University of Pittsburgh) assisted in drafting of figures. Research funding was provided by the U.S. Environmental Protection Agency through the Southwest Center for Environmental Research and Policy.

REFERENCES

ABRAMS, M., 2000, The Advanced Spaceborne Thermal Emission and Reflection Radiometer (ASTER): Data products for the high spatial resolution imager on NASA's Terra platform: *International Journal Remote Sensing,* Vol. 21, pp. 847–859.

BEN-DOR, E.; IRONS, J. R.; AND EPEMA, G. F., 1999, Soil reflectance. In Rencz, A. N. (Editor), *Remote Sensing for the Earth Sciences: Manual of Remote Sensing,* 3rd ed., Vol. 3: John Wiley & Sons, New York, pp. 111–188.

BOTKIN, D. B.; ESTES, J. E.; AND MACDONALD, R. B., 1984, Studying the earth's vegetation from space: *BioScience,* Vol. 34, pp. 508–514.

BROWN, E. R.; MCRAE, J. L.; AND CRAWLEY, A. B., 1989, Effect of aggregates on performance of bituminous concrete. In *Implication of Aggregates in the Design, Construction, and Performance of Flexible Pavements:* American Society of Testing and Materials STP 1016, pp. 34–62.

CHEN, F. AND DUDHIA, J., 2001a, Coupling an advanced land-surface/hydrology model with the Penn State/NCAR MM5 modeling system. Part I: Model implementation and sensitivity: *Monthly Weather Review,* Vol. 129, pp. 569–585.

CHEN, F. AND DUDHIA, J., 2001b, Coupling an advanced land-surface/hydrology model with the Penn State/NCAR MM5 modeling system. Part II: Preliminary model validation: *Monthly Weather Review,* Vol. 129, pp. 587–604.

CHOW, J. C.; WATSON, J. G.; LOWENTHAL, D. H.; SOLOMON, P. A.; MAGLIANO, K.; ZIMAN, S. D.; AND RICHARDS, L. W., 1992, PM10 source apportionment in California's San Joaquin Valley: *Atmospheric Environment,* Vol. 26A, pp. 3335–3353.

CONGALTON, R. G. AND GREEN, K., 1999, *Assessing the Accuracy of Remotely Sensed Data: Principles and Practices:* Lewis Publishers, New York, 137 p.

DANIN, A. AND GANOR, E., 1997, Trapping of airborne dust by Eig's meadowgrass (*Poa eigii*) in the Judean Desert, Israel: *Journal Arid Environments,* Vol. 35, pp. 77–86.

DONNAY, J. P.; BARNSLEY, M. J.; AND LONGLEY, P. A., 2001, Remote sensing and urban analysis. In Donnay, J. P.; Barnsley, M. J.; and Longley, P. A. (Editors), *Remote Sensing and Urban Analysis:* Taylor and Francis, London, pp. 3–18.

ERDAS, 1999, *ERDAS Field Guide,* 5th ed.: ERDAS, Inc., Atlanta, GA, 672 p.

EZEAMUZIE, C. I.; BEG, M. U.; AND AL-AJMI, D., 1998, Responses of alveolar macrophages to post- Gulf-War airborne dust from Kuwait: *Environment International,* Vol. 24, pp. 213–220.

FOODY, G. M., 2000, Estimation of sub-pixel land cover composition in the presence of untrained classes: *Computers Geosciences,* Vol. 26, pp. 469–478.

GANSTER, P.; SWEEDLER, A.; AND CLEMENT, N., 2000, Development, growth, and the future of the border environment. In Ganster, P. (Editor), *The U.S.–Mexican Border Environment: A Road Map to a Sustainable 2020:* San Diego State University Press, San Diego, CA, pp. 73–103.

GEOSYSTEMS GMBH, 1999, *ATCOR2 for ERDAS Imagine User Manual:* Germering, Germany, 81 p.

GÓMEZ, B.; GÓMEZ, M.; SANCHEZ, J. L.; FERNÁNDEZ, R.; AND PALACIOS, M. A., 2001, Platinum and rhodium distribution in airborne particulate matter and road dust: *Science Total Environment,* Vol. 269, pp. 131–144.

GONG, P. AND HOWARTH, P. J., 1990, The use of structural information for improving land-cover classification accuracies at the rural–urban fringe: *Photogrammetric Engineering Remote Sensing,* Vol. 56, pp. 67–73.

HARRIS, P. M. AND VENTURA, S. J., 1995, The integration of geographic data with remotely sensed imagery to improve classification in an urban area: *Photogrammetric Engineering Remote Sensing,* Vol. 61, pp. 993–998.

HEISLER, S.; BALENTINE, H.; BRADLEY, L.; AND GARCIA, M., 1999, *Ambos Nogales Hazardous Air Pollution and Particulate Matter Air Quality Study Final Report:* Arizona Department of Environmental Quality Document 0493-016-300, Phoenix, AZ, 421 p.

HUETE, A. R., 1988, A soil-adjusted vegetation index (SAVI): *Remote Sensing Environment,* Vol. 25, pp. 295–309.

IRISH, R., 1998, *Landsat 7 Data Users Handbook:* Goddard Space Flight Center, MD: http://ltpwww. gsfc.nasa.gov/IAS/handbook/handbook_toc.html.

IRONS, J. R. AND PETERSEN, G. W., 1981, Texture transforms of remote sensing data: *Remote Sensing Environment,* Vol. 11, pp. 359–370.

ISKANDER, F. Y.; VEGA-CARRILLO, H. R.; AND MANZANARES-ACUÑA, E., 1997, Elemental analysis of air dust from Zacatecas City, Mexico: *Environment International,* Vol. 23, pp. 497–506.

JENSEN, J. R., 1996, *Introductory Image Processing: A Remote Sensing Perspective,* 2nd ed.: Prentice-Hall, Upper Saddle River, NJ, 318 p.

KAHLE, A. B.; PALLUCONI, F. D.; AND CHRISTENSEN, P. R., 1993, Thermal

emission spectroscopy: Application to Earth and Mars. In Pieters, C. M. and Englert, P. A. J. (Editors), *Remote Geochemical Analysis: Elemental and Mineralogical Composition:* Cambridge University Press, New York, pp. 99–120.

LANCASTER, N. AND NICKLING, W. G., 1994, Aeolian sediment transport. In Abrahams, A. D. and Parsons, A. J. (Editors), *Geomorphology of Desert Environments:* Chapman & Hall, London, pp. 447–473.

MACMAHON, J. A., 1988, Warm deserts. In Barbour, M. G. and Billings, W. D. (Editors), *North American Terrestrial Vegetation:* Cambridge University Press, New York, pp. 231–264.

MIGUEL, A. G.; CASS, G. R.; GLOVSKY, M. M.; AND WEISS, J., 1999, Allergens in paved road dust and airborne particles: *Environmental Science Technology,* Vol. 33, pp. 4159–4168.

NIEUWENHUIJSEN, M. J.; NODERER, K. S.; SCHENKER, M. B.; VALLYATHAN, V.; AND OLENCHOCK, S., 1999, Personal exposure to dust, endotoxin, and crystalline silica in California agriculture: *Annals Occupational Hygiene,* Vol. 43, pp. 35–42.

PÉWÉ, T. L.; PÉWÉ, E. A.; PÉWÉ, R. H.; JOURNAUX, A.; AND SLATT, R. M., 1981, Desert dust: Characteristics and rates of deposition in central Arizona. In *Desert Dust: Origins, Characteristics, and Effects of Man:* Geological Society of America Special Paper 186, pp. 169–190.

RIDD, M. K., 1995, Exploring a V-I-S (vegetation-impervious surface-soil) model for urban ecosystem analysis through remote sensing: Comparative anatomy for cities: *International Journal Remote Sensing,* Vol. 16, pp. 2165–2185.

SABINS, F. F., 1997, *Remote Sensing: Principles and Interpretation,* 3rd ed.: W.H. Freeman and Company, New York, 494 p.

SCHEFFE, R. D. AND MORRIS, R. E., 1993, A review of the development and application of the Urban Airshed Model: *Atmospheric Environment,* Vol. 27B, pp. 23–39.

SIMCOX, N. J.; FENSKE, R. A.; WOLZ, S. A.; LEE, I.-C.; AND KALMAN, D. A., 1995, Pesticides in household dust and soil: Exposure pathways for children of agricultural families: *Environmental Health Perspectives,* Vol. 103, pp. 1126–1134.

STEFANOV, W. L.; RAMSEY, M. S.; AND CHRISTENSEN, P. R., 2001, Monitoring urban land cover change: An expert system approach to land cover classification of semiarid to arid urban centers: *Remote Sensing Environment,* Vol. 77, pp. 173–185.

STUCKENS, J.; COPPIN, P. R.; AND BAUER, M. E., 2000, Integrating contextual information with per-pixel classification for improved land cover classification: *Remote Sensing Environment,* Vol. 71, pp. 282–296.

TRIETZ, P. M., 1992, Application of satellite and GIS technologies for land-cover and land-use mapping at the rural-urban fringe: A case study: *Photogrammetric Engineering Remote Sensing,* Vol. 58, pp. 439–448.

VOGELMANN, J. E.; SOHL, T.; AND HOWARD, S. M., 1998, Regional characterization of land cover using multiple sources of data: *Photogrammetric Engineering Remote Sensing,* Vol. 64, pp. 45–57.

ZHU, G. AND BLUMBERG, D. G., 2002, Classification using ASTER data and SVM algorithms: The case study of Beer Sheva, Israel: *Remote Sensing Environment,* Vol. 80, pp. 233–240.